THE JOURNAL OF PHYSICAL CHEMISTRY B
A JOURNAL OF THE AMERICAN CHEMICAL SOCIETY

pubs.acs.org/JPCB
Article

Generalized Transition State Theory Treatment of Water-Assisted Proton Transport Processes in Proteins

Published as part of The Journal of Physical Chemistry virtual special issue "Steven G. Boxer Festschrift".

Yu Liu, Chenghan Li, and Gregory A. Voth*

Cite This: *J. Phys. Chem. B* 2022, 126, 10452−10459
Read Online

ACCESS | Metrics & More | Article Recommendations | Supporting Information

ABSTRACT: Transition state theory (TST) is widely employed for estimating the transition rate of a reaction when combined with free energy sampling techniques. A derivation of the transition theory rate expression for a general *n*-dimensional case is presented in this work which specifically focuses on water-assisted proton transfer/transport reactions, especially for protein systems. Our work evaluates the TST prefactor calculated at the transition state dividing surface compared to one sampled, as an approximation, in the reactant state in four case studies of water-assisted proton transport inside membrane proteins and highlights the significant impact of the prefactor position dependence in proton transport processes.

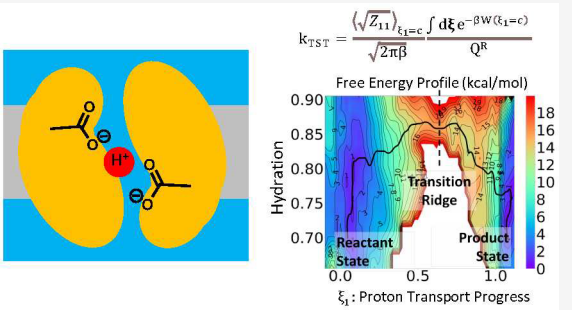

INTRODUCTION

Water is the key solvent in all biological and many chemical reactions and it can play an important role in mediating proton transport (PT). The PT process occurs across a broad range of molecular systems in aqueous solution, from simple acid solutions to complex proteins. The mechanisms associated with PT can be exceedingly intricate and are known to be crucial for proton-coupled transporters, enzymes, and channels,[1,2] wherein the explicit process of PT shows complicated coupling mechanisms to hydration,[3,4] substrate transport,[5] and protein conformational change.[6,7]

Molecular dynamics (MD) simulation can represent a powerful approach for investigating chemical reactions such as PT. In MD, PT is usually taken into account implicitly, such as in MD simulations with empirical classical force fields, or it is treated explicitly via hybrid Quantum Mechanics/Molecular Mechanics[8,9] (QM/MM) or the Multiscale Reactive MD (MS-RMD) method.[10−13] In classical MD simulations, the PT process is considered to occur implicitly between two titratable residues within a protein, or between one titratable residue and water when assigning different protonation states to the protein for separate MD simulations. PT is typically inferred based on analyzing the water network within a confined region of the protein. However, due to the fixed bonding topology of classical MD simulation force fields, the key features of the water-assisted PT, notably the Grotthuss proton hopping[14,15] component of the PT and the explicit correlation[3,4,6,16−24] between water hydration and PT, cannot be described. In contrast, although the most accurate QM/MM MD describes the electronic structure of the QM region explicitly[8] possibly with some treatment to account for nuclear quantum effects[25−28] (NQE), its high computational cost limits the degree of conformational (free energy) sampling and hence the ability to investigate the correlation between water hydration and PT with sufficient statistical sampling.

To overcome these shortcomings of both classical MD and QM/MM, the MS-RMD[10−13,29] reactive MD approach has been developed which can provide both high accuracy and computational speed that is on average 10^3 or more times faster than direct QM/MM. At the same time, MS-RMD also describes the net positive charge defect delocalization associated with the hydrated excess proton[30−32] as well as the Grotthuss hopping nature of the protonic charge defect.[33]

Due to the initial high thermodynamic barrier (5−20 kcal/mol) for proton transfer between weak acids/bases and the accepting water molecule(s), both QM/MM and MS-RMD require a combination of free energy sampling techniques to draw an accurate picture of the PT process with statistically meaningful results and within accessible simulation time. Free energy sampling approaches such as umbrella sampling[34] and metadynamics[35−40] require a predefined reaction coordinate, more recently called a "collective variable" (CV), that provides a mathematical measure of the reaction progress. Most commonly, molecular dynamics sampling is used to average out the orthogonal degrees of freedom (DOF) into the free

Received: September 20, 2022
Revised: November 15, 2022
Published: December 2, 2022

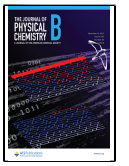

https://doi.org/10.1021/acs.jpcb.2c06703
J. Phys. Chem. B 2022, 126, 10452−10459

energy profile, the so-called potential of mean force (PMF). As a result, to begin to describe a water-assisted PT process within a protein, the location of the transported Grotthuss hopping excess proton charge defect must be tracked. As will be discussed later, in many cases one must also sample a water hydration CV, which ideally also describes the functional connectivity of the proton transporting water chain.[4]

An initial concept of an excess proton tracker was established in the 1990s as the overall dipole movement of the water chain.[41,42] As later reported,[43] this initial proton tracker, which is defined as a linear combination of atomic coordinates, is greatly influenced by the permanent dipole movement of the fluctuating water molecules far from the PT active center, making it a less appropriate proton tracker. A more recent concept for the excess proton tracker is commonly known as the center of excess charge (CEC). All CEC definitions (MS-RMD CEC,[44] rCEC,[13,45] mCEC,[43] and the "proton indicator"[46]) adopt a nonlinear form of the atomic coordinates to capture the delocalized nature of the excess proton charge defect and the chemically reactive (Grotthuss hopping) nature of PT, while minimizing the environmental water dipole contamination described earlier. To describe the progress of PT within a protein, the CV is usually defined as a function of the distance between the CEC position and the site of interest (e.g., protein amino acid residue or substrate). Due to the curvilinear CEC CV expression, all forms of PT CV designed for a water-assisted PT process do not, therefore, correspond to a linear combination of the atomic coordinates of the system. As we will discuss in more detail, a curvilinear CV employed in TST produces a nontrivial prefactor in the form of a statistical ensemble average.

Other coupled DOF such as substrate transport, the PT pathway hydration process (noted earlier), and local protein conformational changes can also be slow and therefore critical to the PT process.[3,4,6,16−24] In such cases, additional CVs are necessary to be explicitly expressed in the free energy sampling process to reflect coupling of PT to those DOFs, along with the CEC describing the PT CV, thereby giving a more complex PMF for the coupled PT process having two dimensions or more. However, if such a PMF can be obtained (or if 1D for just the CEC is sufficient), then with the application of transition state theory (TST),[47,48] a transition rate can be directly estimated for the PT process from PMF data.

Conventional TST predicts an upper bound to the reaction rate of the system. The upper bound arises from the nonrecrossing assumption of a hypersurface that divides the phase space into the reactant and the product regions; i.e., a successful reaction will take place once the system reaches the transition state. There are two critical components in the TST formalism: the first is the exponential dependence of the reactant minimum to transition state free energy barrier,[49] while the second is the prefactor related, in essence, to the velocity of the effective mass of the CV as it crosses the dividing surface.

Previous research has presented derivations of the mass-dependent prefactor expression for 1D rate constants for general curvilinear CVs[48,50] and applications for both rectilinear[51,52] and curvilinear[53] CVs with associated PMFs. However, the definition of the water-assisted PT CV, with its effective mass intrinsically dependent on the sampling position of the PMF, requires a more detailed and specific study with respect to the impact of the mass prefactor on the rate expression. Building on prior research,[48] the present study extends the mass prefactor expression in terms of a dividing surface on a 2D PMF as a function of both a general curvilinear PT CV and a hydration-related CV. As discussed herein, we develop an exact form of the expression for the mass prefactor for a general n-dimensional case and then study various approximations to the TST transition-rate constant for both 1D and 2D examples of water-assisted PT processes in proteins. Our results confirm the importance of the phase-space position-dependence of the mass prefactor for water-assisted PT processes and establishes a standard protocol for applying this methodology in future research.

METHODS

Rate Constant Expressions in Generalized Transition State Theory. The TST rate constant expression in a general form for the reaction CV, $\boldsymbol{\xi}$, and with a dividing surface described by $\boldsymbol{\xi} = \mathbf{s}(\mathbf{r})$ in the context of a PMF is given by

$$k_{\mathrm{TST}} = \frac{1}{\mathrm{Q}^{\mathrm{R}}} \int \frac{\mathrm{d}\mathbf{r}\mathrm{d}\mathbf{p}}{h^{3\mathrm{N}}} \delta(\xi - s(\mathbf{r})) \Theta(\dot{\xi}_{\mathrm{ver}}) \dot{\xi}_{\mathrm{ver}}\, \mathrm{e}^{-\beta \mathrm{H}} \tag{1}$$

where $\mathbf{r}$ are the 3N atomic coordinates of the system, $\mathbf{p}$ are the conjugate linear momentum, N is the total number of the atoms in the system, and $\mathbf{s}(\mathbf{r})$ is the transition state dividing manifold. Q^{R} is the reactant partition function and can be calculated from the integral of the Boltzmann factor over the reactant phase space. Note that $\dot{\xi}_{\mathrm{ver}}$ is the vertical velocity component of $\boldsymbol{\xi}$ to the transition ridge; then according to TST, this factor contributes to the forward reaction flux when found to be a positive value. This relationship is expressed by the step function $\theta(\dot{\xi}_{\mathrm{ver}})$ in the expression.

Once one transforms the 3N dimensional vector $\mathbf{r}$ to $\boldsymbol{\xi}$, the 3N-n dimensional vector $\mathbf{q}$ can be chosen such that no cross terms in the momentum expression between $\mathbf{p}_{\xi}$ and $\mathbf{p}_{\mathrm{q}}$ remains. The Hamiltonian of the system is then given by

$$\mathrm{H} = \frac{1}{2}\mathbf{p}_{\xi}^{\mathrm{T}}\mathbf{Z}_{\xi}\mathbf{p}_{\xi} + \frac{1}{2}\mathbf{p}_{q}^{\mathrm{T}}\mathbf{Z}_{q}\mathbf{p}_{q} + \mathrm{V}(\boldsymbol{\xi}, \mathbf{q}) \tag{2}$$

where $\mathbf{Z}_{\boldsymbol{\xi}}$ is the inverse of the effective mass of the CV ξ such that

$$(\mathbf{Z}_{\xi})_{jk} := \sum_{i=1}^{3\mathrm{N}} \frac{1}{\mathrm{M}_i} \left(\frac{\partial \xi_j}{\partial \mathrm{r}_i}\right)\left(\frac{\partial \xi_k}{\partial \mathrm{r}_i}\right) \tag{3}$$

and $\mathrm{V}(\boldsymbol{\xi}, \mathbf{q})$ is the potential energy expressed as a function of transformed coordinates ξ and $\mathbf{q}$.

Previously, Schenter et al.[48] derived the TST rate constant expression on the 1D PMF $\mathrm{W}(\boldsymbol{\xi})$, as a function of a general curvilinear CV, given by

$$k_{\mathrm{TST}} = \frac{\langle \sqrt{\mathrm{Z}_{\xi}} \rangle_{\xi=\xi^{\mathrm{TS}}}}{\sqrt{2\pi\beta}} \frac{\mathrm{e}^{-\beta \mathrm{W}(\xi^{\mathrm{TS}})}}{\mathrm{Q}^{\mathrm{R}}} \tag{4}$$

This equation provides an accurate expression for the transition-rate prefactor with an effective mass factor expression $\langle \sqrt{\mathrm{Z}_{\xi}} \rangle_{\xi=\xi^{\mathrm{TS}}}$, which is the ensemble average value of $\sqrt{\mathrm{Z}_{\xi}}$ sampled at the transition state.

Inspired by the work of Schenter et al, we have derived the TST rate constant expression for an n-dimensional PMF with a set of general curvilinear CVs, $\boldsymbol{\xi}$, here we assume the dividing surface can be described as $\boldsymbol{\xi}_1 = \boldsymbol{\xi}_{\mathrm{TS}}$. This may be always achieved by a nonlinear transformation of ξ such that the

https://doi.org/10.1021/acs.jpcb.2c06703
J. Phys. Chem. B 2022, 126, 10452−10459

generally nonlinear $\mathbf{s}(\mathbf{r})$ manifold becomes a hyper-plane and choosing its normal direction as $\boldsymbol{\xi}_1$. Practically, we found such a transformation is not needed for our case studies. The PT CV was found to already satisfy this assumption as evidenced by the fact that a vertical line approximates well the transition ridge on the 2D-PMFs as shown in the next section. The rate expression in terms of a n-dimensional PMF $W(\boldsymbol{\xi})$ is then given by

$$k_{\mathrm{TST}} = \frac{\langle\sqrt{\mathrm{Z}_{11}}\rangle_{\xi_1=\xi_{\mathrm{TS}}}}{\sqrt{2\pi\beta}} \frac{\int \mathrm{d}\boldsymbol{\xi}\ \mathrm{e}^{-\beta \mathrm{W}(\xi)}\delta(\xi_1 - \xi_{\mathrm{TS}})}{\mathrm{Q}^{\mathrm{R}}} \tag{5}$$

in which the mass factor $\langle\sqrt{\mathrm{Z}_{11}}\rangle_{\xi_1=\xi_{\mathrm{TS}}}$ is the ensemble average of $\sqrt{\mathrm{Z}_{11}}$ along the rectilinear transition ridge of the PMF $\boldsymbol{\xi}_1 = \boldsymbol{\xi}_{\mathrm{TS}}$ and the expression of Z is given in eq 3. Note that the mass factor expression in eq 5 is only dependent on $\boldsymbol{\xi}_1$ (regardless of the other $\boldsymbol{\xi}$'s expression) due to the transition ridge approximation. This derivation is provided in SI.

Approximation for Mass Factor in Transition State Theory. Approximations in prior literature have often employed the sampled mass factor from the simulation trajectories corresponding to the reactant state, instead of at the transition state on either 1D or 2D PMFs. An example of this can be found in studies of the water-assisted PT process within a protein.[6,19−21,23,54] This approximation simply amounts to the following expression,

$$\langle\sqrt{\mathrm{Z}_{11}}\rangle_{\xi=\xi_{\mathrm{TS}}} \approx \langle\sqrt{\mathrm{Z}_{11}}\rangle_{\xi=\xi_{\mathrm{R}}} \tag{6}$$

The approximation stated in eq 6 becomes exact if $\boldsymbol{\xi}_1$ is a linear function of atomic coordinates, such that $\frac{\partial\xi_1}{\partial r_i}$ is constant and does not depend on the atom positions. An example of such a CV is the center of mass of a protein. The approximation could still be valid for some curvilinear CVs, if the value of Z_{11} is constant or insensitive along the minimum free energy path. Examples of such a CV are a pairwise distance or a simple proton transfer coordinate, $r_{\mathrm{HA}} - r_{\mathrm{HB}}$, where A/B are proton donor/acceptor atoms. We note that, as long as the ensemble average of $\sqrt{\mathrm{Z}_{11}}$ is evaluated correctly, this approximation does not rely on the linearity in CVs other than $\boldsymbol{\xi}_1$.

Moreover, this prior approximation has sometimes utilized the equipartition theorem, by stating that

$$\langle\sqrt{\mathrm{Z}_{11}}\rangle \approx \sqrt{\langle\mathrm{Z}_{11}\rangle} \approx \sqrt{\beta\langle\dot{\xi}_1^2\rangle} \tag{7}$$

The first part of the second approximation stated in eq 7, $\langle\sqrt{\mathrm{Z}_{11}}\rangle \approx \sqrt{\langle\mathrm{Z}_{11}\rangle}$, is valid when Z_{11} approximates a constant, and thus, the conditions we discussed about the first approximation also apply here. Although those conditions are sufficient for $\langle\sqrt{\mathrm{Z}_{11}}\rangle \approx \sqrt{\langle\mathrm{Z}_{11}\rangle}$ to be true, they are usually not necessary conditions. It can be seen, from $\mathrm{var}(\sqrt{\mathrm{Z}_{11}}) = \langle\mathrm{Z}_{11}\rangle - \langle\sqrt{\mathrm{Z}_{11}}\rangle^2$ that the quality of this approximation is related to the intrinsic fluctuation of $\sqrt{\mathrm{Z}_{11}}$. The equipartition theorem used in the second part of the approximation, $\langle\mathrm{Z}_{11}\rangle = \beta\langle\dot{\xi}_1^2\rangle$, is exact (see the proof in the Supporting Information, SI). Due to the greater sampling of $\dot{\xi}_1$ (since it can be computed from finite difference upon $\boldsymbol{\xi}_1$ time series), and due to $\beta\langle\dot{\xi}_1^2\rangle$ being used in the previous literature, we only report here $\beta\langle\dot{\xi}_1^2\rangle$ values.

Ab Initio MD (AIMD) and MS-RMD CV Definitions for Water-Assisted Proton Transport. Here, we briefly explain the mCEC[43] and rCEC[45] definitions that have been used as a PT CV in AIMD (and also QM/MM) simulations, as well as the MS-RMD CEC CV in MS-RMD simulations. This is followed by a discussion of the nonlinear properties of the CEC definition function itself with respect to atomic coordinates. The mCEC is defined as

$$r_{\mathrm{mCEC}} = \sum_{i\in\{\mathrm{H}\}} r_i - \sum_{j\in\{\mathrm{X}\}} w_j r_j - \sum_{i\in\{\mathrm{H}\}}\sum_{j\in\{\mathrm{X}\}} f_{\mathrm{sw}}(r_{ij})(r_i - r_j)$$
$$f_{\mathrm{sw}}(r_{ij}) = \frac{1}{1 + \exp\frac{r_{ij} - r_0}{d_0}} \tag{8}$$

where $\{\mathrm{H}\}$ is the collection of hydrogen atoms and $\{\mathrm{X}\}$ is the collection of heavy atoms in the AIMD (or QM/MM) description of the system. The weighting factor w_j is assigned as the number of protons originally bonded to the heavy atom j prior to the acceptance of the proton. For example, the weighting factor of Asp and Glu side chain oxygens is 0, and the weighting factor of the water oxygen is 2. The switching function $f_{\mathrm{sw}}(r_{ij})$ employed a Fermi function form with parameter r_0 and d_0 to allow a smooth transition between 0 and 1, which corresponds to the nonbonding and bonding state of each proton-heavy atom pair ij. Taking a Zundel cation $\mathrm{H_5O_2^+}$ pair as an example, when proton stays between two water molecules, $f_{\mathrm{sw}}(r_{\mathrm{ij}})$ of each hydrogen−oxygen pair becomes 1 (except for the atomic pair of shared hydrogen with oxygen, switching function becomes 0.5). The water "dipole moment" $(r_{\mathrm{H1}} + r_{\mathrm{H2}} - 2r_{\mathrm{O1}})$ from the first two terms of eq 8 was canceled by the third term due to the pairwise switching function corresponding to $\mathrm{H_1}-\mathrm{O_1}$ and $\mathrm{H_2}-\mathrm{O_1}$ pairs. The switching function does not require any additional normalization factor since this expression is normalized upon construction. More explicitly, the coefficient of all atoms should be exactly 1. The nonlinear property of the mCEC function with respect to the atomic coordinates of the system arises merely from the switching function $f_{\mathrm{sw}}(r_{\mathrm{ij}})$.

The rCEC employs the diabatic state concept in MS-RMD theory, where it is defined as

$$r_{\mathrm{rCEC}} = \sum_{i\in\{\mathrm{I}\}} c_i^2 \mathrm{r}_i^{\mathrm{COC}} \tag{9}$$

and $\{\mathrm{I}\}$ denotes the collection of all possible diabatic states of the system, and $r_{\mathrm{i}}^{\mathrm{COC}}$ is the position of the center of excess charge of the protonated species in the fixed bonding topology of the ith RMD diabatic state

$$r_i^{\mathrm{COC}} = \frac{\sum_j |q_j| r_j}{\sum_j |q_j|} \tag{10}$$

where j runs over all atoms in the protonated molecule (e.g., all carboxylic hydroxyl atoms in the protonated aspartate or glutamate acid, or all four atoms in the hydronium).

The probability of the system remaining in the diabatic state I is denoted as c_i^2. The approximation made for c_i^2 is as follows,

$$\frac{c_j^2}{c_i^2} = \exp(-\mathrm{k}(\delta_{ijk} - \delta_0)) \tag{11}$$

https://doi.org/10.1021/acs.jpcb.2c06703
J. Phys. Chem. B 2022, 126, 10452−10459

$$\sum_{i\in\{I\}} c_i^2 = 1 \tag{12}$$

where the proton-sharing indicator, $\delta_{ijk} = r_{jk} - r_{ik}$, corresponds to the extent of proton sharing (indicated as k) between the two diabatic state protonated species. The positive δ_{ijk} indicates the proton to be predominantly held by the protonated molecule in diabatic state i, while negative δ_{ijk} indicates the proton to be predominantly held by the protonated molecule in diabatic state j. The term r_{jk} represents the distance between the proton and the oxygen of the proton acceptor in diabatic state i. Like mCEC, the rCEC function shows a nonlinear dependence with respect to the atomic coordinates of the system due to the nonlinear dependence of the probability c_i^2 of diabatic state $|i\rangle$ to the atomic coordinates of the system.

The MS-RMD CEC, noted just as CEC here, shares the same expression as the rCEC, except for the definition of c_i. In the MS-RMD framework, the ground state of the system $|\psi\rangle$ can be expressed as a linear combination of distinct bonding topologies $|i\rangle$ or diabatic states. The expansion coefficient of the ground state in relation to the diabatic state $|i\rangle$ is defined as c_I, so the total linear combination is given by

$$|\psi\rangle = \sum_i c_i|i\rangle \tag{13}$$

The c_i's are calculated on the fly during the RMD simulation by solving the eigenvalue problem with the Hamiltonian of the system, expressed as $H = \sum_{ij} h_{ij}|i\rangle\langle j|$, such that

$$\mathbf{Hc} = E_0\mathbf{c} \tag{14}$$

Here, h_{ii} is the potential energy of the system within the diabatic state $|i\rangle$, and h_{ij} is the coupling energy between diabatic states $|i\rangle$ and $|j\rangle$. E_0 is the solved eigenvalue corresponding to the ground state energy of the system as a function of all coordinates, and $\mathbf{c}$ is the ground state eigenvector from the diabatic-state basis set. It should be noted that the MS-RMD CEC function is not a linear-combination of atomic coordinates of the system as the on-the-fly solved ground state eigenvector $\mathbf{c}$ depends on those coordinates nonlinearly.

Effective TST Mass Factor for Water-Assisted Proton Transport. The mass factor in the TST rate expression for both 1D and 2D PMFs is based on the derivative of the proton-transfer CV to the atomic coordinates within, e.g., a protein−water-substrate complex. Since the CEC incorporated within the PT CV is already a curvilinear function of atomic coordinates, the derivative value of the PT CV as a function of the atomic coordinates will vary based on the value of the CV. Thus, one can expect the ensemble average of $\sqrt{Z_\xi}$ sampled at a given reactant state to display a significant difference in magnitude in comparison to the (correct) one sampled at the transition state for a PT process, e.g., in proteins.

RESULTS AND DISCUSSION

1D TST Results. The exact form of the TST expression for the effective mass factor was employed here for 1D PMFs of water assisted PT in two proton-coupled transporters.[5,54] The impact of the approximations on the value of the mass factor was studied and compared to the exact value.

The *Piriformospora indica* phosphate transporter[55] (PiPT) is a proton-coupled phosphate transporter within the major facilitator superfamily[56] (MFS). The coupling relationship between PT and phosphate transport was studied in our recent work[5] via extensive classical simulations and QM/MM MD. The collective variable $\boldsymbol{\xi}$ that describes the PT from D324 to D45 in the QM/MM MD PMF (Figure 1A) is defined as a curvilinear function of multiple distances between AIMD rCEC, phosphate, D324 and D45 side chain oxygens, such that

$$\xi = \vec{r}_{\mathrm{CEC-Pi}} \cdot \frac{\vec{r}_{\mathrm{D324-D45}}}{|\vec{r}_{\mathrm{D324-D45}}|} \tag{15}$$

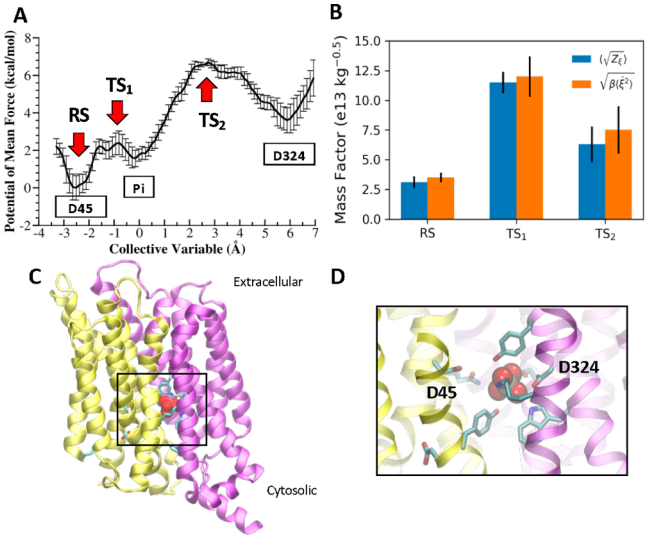

Figure 1. QM/MM MD proton transfer PMF in PiPT. (A) The potential of mean force (PMF) of the PT process staring from D324 to D45 via waters and phosphate titration events. RS indicates the reactant state, TS_1 and TS_2 correspond to the transition states for the PT process from D45 to Pi and from D45 to D324. (B) Calculated mass factor at different locations of the PMF stated in (A) with the exact approach and the equipartition approach from the trajectories of the earlier work[5] (error bars are solid black lines). (C) Side view of the PiPT protein crystal structure with phosphate bonded; the N domain helices are marked in yellow, and C domain marked in purple. (D) Enlarged view of the PT local environment with nearby residues represented as sticks and phosphate represented in sphere representation.

The calculated mass factor using the exact expression $\langle\sqrt{Z_\xi}\rangle_\xi = \left\langle \sum_{i=1}^{3N} \frac{1}{M_i}\left(\frac{\partial\xi}{\partial r_i}\right)^2 \right\rangle_\xi$ and the equipartition expression $\langle\sqrt{Z_\xi}\rangle_\xi = \sqrt{\beta\langle\dot{\xi}\rangle_\xi}$ sampled at both the reactant state and transition states in the PMF are provided in the chart of Figure 1B. Note that the orange and blue bars, which correspond to the exact and approximate equipartition approach, respectively, do not show evidence of a marked difference in the calculated value of the mass factor. However, there is a non-negligible dependence of the mass factor and the position in the PMF when sampling the ensemble average. As shown in the chart, the calculated TST rate constant with these effective mass factors can be different by a factor as large as 4, which borders on a serious difference.

We then compared the mass factor values from calculated from the different approaches for a proton-coupled peptide transporter, $PepT_{xc}$, in the peptide oligomer transporter family.[57] Our earlier computational work[58] incorporated

https://doi.org/10.1021/acs.jpcb.2c06703
J. Phys. Chem. B 2022, 126, 10452−10459

QM/MM MD combined with enhanced free energy sampling techniques to determine the PT event that effects the inward-open to outward-open conformational transition of the protein. The PMF shown in Figure 2A is for the PT process from D322 to E425, which was suggested to trigger the conformational transition of the transporter.

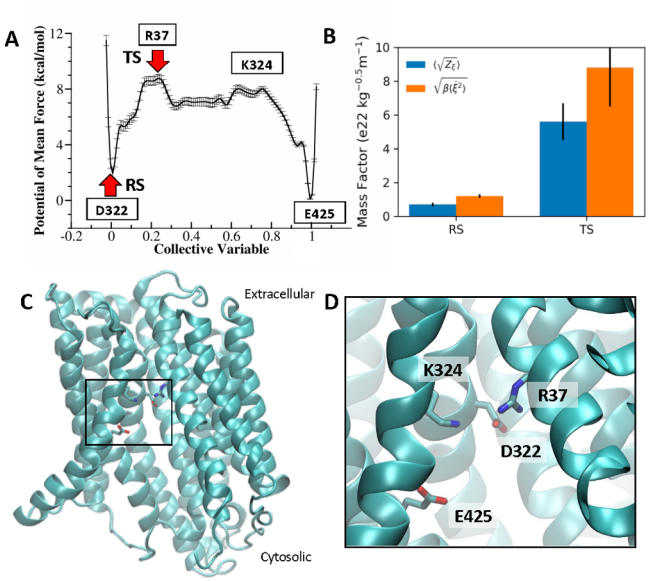

Figure 2. QM/MM MD proton transfer PMF in PepT. (A) Potential of mean force (PMF) of the PT process stating from D322 to E425 via water wires. (B) Calculated mass factor at reactant state and the transition state of the PMF stated in (A) with the exact approach and the equipartition approach from the trajectories of the earlier work.[58] (C) Side view of the PepT structure inside the membrane. (D) Enlarged view of the PT local environment with nearby residues represented as sticks.

The collective variable ξ that describes the PT from D322 to E425 in the QM/MM MD PMF (Figure 2A) is defined as the ratio of distances between the projected value of distance between the AIMD mCEC and D322 and the distance between D322 to E425 side chain oxygens.

$$\xi = \frac{r_{\mathrm{CEC-D}} \cos \angle(\mathrm{CEC-D-E})}{r_{\mathrm{DE}}} \tag{16}$$

The *m*CEC marks the position of the proton, and r_{DE} and $r_{\mathrm{CEC-D}}$ denote the distance between D322 and E425 and the distance between D322 and the excess proton position, respectively.

The calculated mass factor using the exact expression $\langle\sqrt{Z_\xi}\rangle_\xi = \left\langle \sum_{i=1}^{3N} \frac{1}{M_i}\left(\frac{\partial\xi}{\partial r_i}\right)^2 \right\rangle_\xi$ and the equipartition expression $\langle\sqrt{Z_\xi}\rangle_\xi = \sqrt{\beta\langle\dot{\xi}\rangle_\xi}$ sampled in the reactant state and at the transition states in the PMF are provided in Figure 2B. Note that the calculated mass factors exhibit a strong contrast between different sampling positions in the PMF, with the transition state mass factor being 7 times greater than the analogous reactant state value. Observed differences in the mass factor values calculated using the two methods were found to be marginally statistically significant; however the difference of the effective mass factor calculated (correctly) at the transition state versus in the reactant well is still quite large, on the order of a factor of 5−8.

2D TST Results and the Role of Hydration as a Second CV. When the PT occurs throughout a pore or an otherwise narrow pathway within the protein, it is likely that the dynamics of the hydration process are strongly coupled with different stages of the PT charge translocation event.[4] Such cases can be identified from postanalysis of trajectories involving explicit PT, as each will show a distinct excess proton CEC position along its transport pathway. When there is a clear dependency between the trend of some water hydration indicator and different stages of the PT CV, either the water connectivity or the water density of the PT pathway needs to be additionally sampled as a CV to accurately capture the PT process.

Below, we have applied a derived 2D TST expression (eq 5; for derivation, see the SI) to calculate the effective TST mass factor at different positions along the 2D PT PMF of the two protein systems. The ratio between this quantity in the reactant state and the transition ridge indicates the extent to which prior approximations will impact the mass factor of the TST constant as the correct answer is the one involving the calculation at the transition ridge.

ClC-ec1 (Figure 3) is a chloride-proton antiporter that also transports multiple anions with a distinct stoichiometry factor

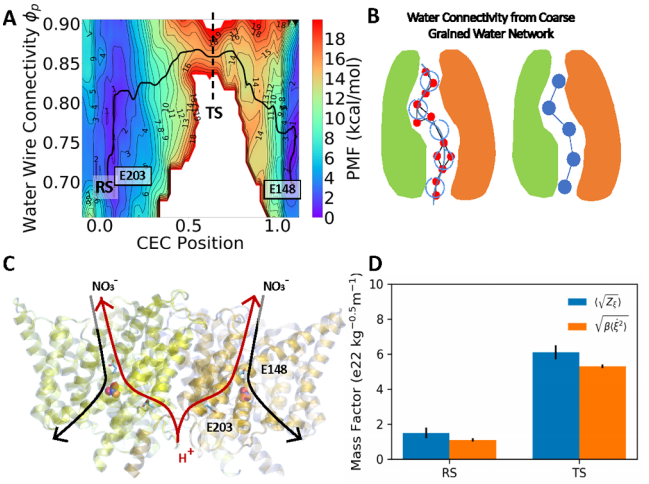

Figure 3. MS-RMD PT PMF in ClC-ec1 dimer. (A) Potential of mean force (PMF) of the PT process starting from E203 to E148 with a nitrate anion bound in the vicinity. (B) Schematic of the water wire connectivity CV. (C) Side view of the ClC-ec1 dimeric structure within the membrane with nitrate in a VDW representation. (D) Calculated mass factor at the reactant state and the transition state of the PMF shown in (A) with different calculated effective mass approaches based on trajectories from earlier work.[4]

for each transported anion. Extensive experiments have been done in the past to interpret the cotransport mechanisms for each type of anion. Additionally, our prior computational studies[19−22,59,60] have employed a range of approaches to analyze the molecular-level anion modulation mechanism with respect to PT. In general, the MS-RMD approach was proven to be a most suitable method for studying the explicit PT mechanisms as affected by different stages of the anion transport, with a crucial consideration of the proton-induced hydration effect.

https://doi.org/10.1021/acs.jpcb.2c06703
J. Phys. Chem. B 2022, 126, 10452−10459

The proton transport progress in the free energy landscape (Figure 3A) utilizes a novel hydration indicator CV, the water connectivity (Figure 3B), combining graph theory and a coarse-grained representation of the water network within the protein (Figure 3C).[4] Based on specifying the starting and end points of the water network, this water connectivity CV quantifies the extent of connectivity of the most-connected water wire associated with the explicit PT process. Here, the MS-RMD CEC was also employed to track the location of the transported excess proton charge defect on the fly, while the horizontal PT CV on the PMF, denoted by ξ, is denoted by the relative position of the excess proton CEC compared to the projected distance of the two Glu residues E203 and E148 along the direction perpendicular to the membrane plane. The expression of ξ is as follows,

$$\xi = \frac{\min\limits_{i\in\{1,2\}} (\mathbf{r}_{CEC} - \mathbf{r}_{E203,i})\cdot\widehat{\mathbf{n}_{PT}}}{\min\limits_{i,j\in\{1,2\}} (\mathbf{r}_{E148,j} - \mathbf{r}_{E203,i})\cdot\widehat{\mathbf{n}_{PT}}} \tag{17}$$

where $\widehat{\mathbf{n}_{PT}}$ is a predefined unit vector pointing from E203 to E148, $\mathbf{r}_{CEC}$, $\mathbf{r}_{E203,i}$, $\mathbf{r}_{E148,j}$ are the coordinates of the MS-RMD CEC position, the ith carboxyl oxygen of E203 and the jth carboxyl oxygen of E148. From the derived expression in the SI and with an assumption of a rectilinear transition ridge parallel to the second CV of the PMF, the mass factor for the transition-rate constant is independent of the gradient of the water connectivity CV to atomic coordinates in the system. The calculated mass factor from the derived exact form of the TST expression at the transition ridge ensemble in Figure 3D presents a 4:1 ratio to the one calculated in the reactant basin, which again highlights the significant flaw in the assumption that the PT CV will adopt the same effective mass between the reactant basin and the transition ridge in the PMF.

The sarcoplasmic reticulum Ca^{2+}-ATPase pump (SERCA, Figure 4) belongs to the P-type ATPase family, which carries out calcium-cation transport in cells to enable muscle contraction and maintain intracellular Ca^{2+} homeostasis. Additionally, SERCA transports multiple protons in the opposite direction of the outflow of Ca^{2+} in the endoplasmic reticulum/sarcoplasmic reticulum domain and is found to colocalize with several chloride-channel (ClC) family proteins. Our recent computational study[23] of explicit PT process in SERCA via the MS-RMD approach along with free energy sampling techniques confirmed the feasibility of PT from E908 to the luminal side.

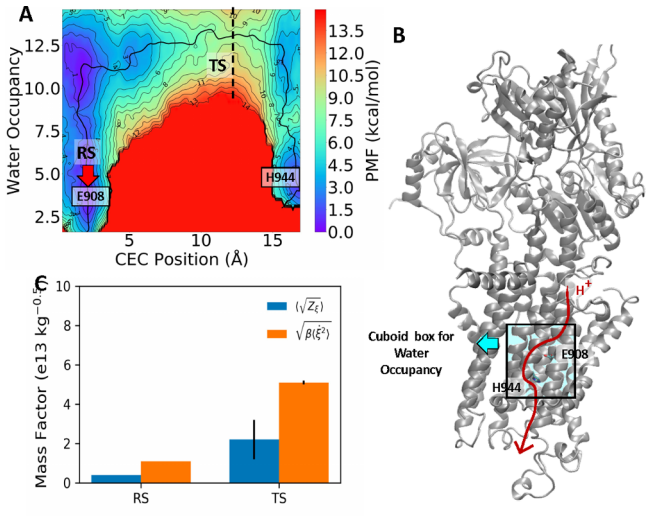

Figure 4. MS-RMD PT PMF in SERCA. (A) Potential of mean force (PMF) of the PT process staring from E908 to H944. (B) Side view of the protein within the membrane; the red arrow points to the direction of PT within the protein across the membrane. The black box highlights the cuboid box boundary for the water occupancy CV. (C) Calculated mass factor at the reactant state and the transition state of the PMF as seen in (A) with different calculation approaches from the trajectories taken from earlier work.[23]

The 2D MS-RMD PMF obtained via umbrella sampling (Figure 4A) illustrates PT from E908 to the H944 residue inside SERCA. The horizontal PT CV is defined as the projection of the MS-RMD CEC position along a curvilinear path. The discrete CV points that define the path were obtained from the sampled configurations from a Metadynamics[35−38] run. The water occupancy within the cuboid box (shown in Figure 4B) was employed as the second CV for free energy sampling to capture the couple water hydration response to the excess proton position. The calculated TST effective mass factor calculated from either the exact form of the expression or the equipartition assumption expression sampled at either the reactant and (correctly) at the transition ridge on the PMF once again displays a difference of about a factor of 4 (Figure 4C). We note that the discrepancy in the mass factor value calculated by the two different methods was found to be a result from the postanalysis of the velocity of the first CV and the assumption of $\langle\sqrt{Z_\xi}\rangle_\xi = \sqrt{\langle Z_\xi\rangle_\xi}$.

CONCLUSIONS

A prefactor ratio of order 3−10 is considered to be significantly important in both a practical and a fundamental sense as the TST rate is proportional to the prefactor value. The statistical error of the reaction PMF calculation can also be important for $e^{-\beta W(\xi^{TS})}$ in eq 4 which constitutes the overall TST rate constant value. The 1D PMF and 2D PMF error profiles are all around k_BT in this work and this statistical error contribution from the free energy barrier can be estimated as $\exp -\beta\Delta W = \exp(\pm 1)$, thus ranging from 0.4 to 2.7 times to the overall TST rate value. The impact of the statistical error in the PMF can therefore be as important as the impact of any prefactor approximation in the overall TST rate calculation, but of course the PMF statistical error can always be better converged numerically whereas a systematic error in the calculation of the TST prefactor cannot be eliminated. Moreover, all approximations to the prefactor calculation will share the same calculated PMF. The correct manner of calculating the prefactor therefore matters for obtaining a correct overall TST rate value given a PMF of a given statistical significance.

In this work, we have derived the exact form of TST for the general n-dimensional case with curvilinear CVs and applied this approach to calculate the effective mass factor for PT reactions (with and without coupled hydration) in several biomolecular systems. These four applications to water-assisted PT within selected proteins exhibit up to nearly an order of magnitude difference in value between the actual (correct) effective mass factor calculated at the transition state dividing surface compared to one sampled, as an approximation, in the reactant state for 1D and 2D PMFs. Interestingly, the mass factor calculation was relatively insensitive to using an equipartition approximation. Our results thus highlight the significant impact of the position dependence of the effective

https://doi.org/10.1021/acs.jpcb.2c06703
J. Phys. Chem. B 2022, 126, 10452−10459

mass factor in TST for PT processes and one that should not be taken lightly if quantitative accuracy is the goal in the calculated TST rate constant. The results described herein are therefore expected to provide a more accurate basis for the prediction of the PT rate in future studies of PT in biomolecular and other systems.

■ ASSOCIATED CONTENT

Supporting Information

The Supporting Information is available free of charge at https://pubs.acs.org/doi/10.1021/acs.jpcb.2c06703.

Derivation of transition state rate constant in terms of an n-dimensional PMF; calculation details of the ensemble average of $\langle\sqrt{Z_\xi}\rangle$ among transition states in terms of a 2D PMF; proof of the equipartition theorem $\langle Z_{11}\rangle = \beta\langle\dot{\xi}_1^2\rangle$ in terms of an n-dimensional PMF (PDF)

■ AUTHOR INFORMATION

Corresponding Author

Gregory A. Voth − *Department of Chemistry, Chicago Center for Theoretical Chemistry, James Franck Institute, and Institute for Biophysical Dynamics, The University of Chicago, Chicago, Illinois 60637, United States;* orcid.org/0000-0002-3267-6748; Email: gavoth@uchicago.edu

Authors

Yu Liu − *Department of Chemistry, Chicago Center for Theoretical Chemistry, James Franck Institute, and Institute for Biophysical Dynamics, The University of Chicago, Chicago, Illinois 60637, United States*

Chenghan Li − *Department of Chemistry, Chicago Center for Theoretical Chemistry, James Franck Institute, and Institute for Biophysical Dynamics, The University of Chicago, Chicago, Illinois 60637, United States*

Complete contact information is available at: https://pubs.acs.org/10.1021/acs.jpcb.2c06703

Notes

The authors declare no competing financial interest.

■ ACKNOWLEDGMENTS

This research was supported by the National Institute of General Medical Sciences (NIGMS) of the National Institutes of Health (NIH) through grant R01 GM053148. We thank Drs. Santanu Roy at Oak Ridge National Laboratory, Gregory K. Schenter and Christopher J. Mundy of Pacific Northwest National Laboratory, and Han Feng at Berkely for their insights and valuable discussion. Computational resources were provided by the Extreme Science and Engineering Discovery Environment (XSEDE), which is supported by National Science Foundation Grant OCI-1053575 and the University of Chicago Research Computing Center (RCC).

■ REFERENCES

(1) Decoursey, T. E. Voltage-Gated Proton Channels and Other Proton Transfer Pathways. *Physiol. Rev.* **2003**, *83* (2), 475−579.

(2) Wraight, C. A. Chance and design—Proton transfer in water, channels and bioenergetic proteins. *Biochimica et Biophysica Acta (BBA) - Bioenergetics* **2006**, *1757* (8), 886−912.

(3) Peng, Y.; Swanson, J. M. J.; Kang, S.-g.; Zhou, R.; Voth, G. A. Hydrated Excess Protons Can Create Their Own Water Wires. *J. Phys. Chem. B* **2015**, *119* (29), 9212−9218.

(4) Li, C.; Voth, G. A. A quantitative paradigm for water-assisted proton transport through proteins and other confined spaces. *Proc. Natl. Acad. Sci. U. S. A.* **2021**, *118* (49), No. e2113141118.

(5) Liu, Y.; Li, C.; Gupta, M.; Verma, N.; Johri, A. K.; Stroud, R. M.; Voth, G. A. Key computational findings reveal proton transfer as driving the functional cycle in the phosphate transporter PiPT. *Proc. Natl. Acad. Sci. U. S. A.* **2021**, *118* (25), No. e2101932118.

(6) Liang, R.; Li, H.; Swanson, J. M.; Voth, G. A. Multiscale simulation reveals a multifaceted mechanism of proton permeation through the influenza A M2 proton channel. *Proc. Natl. Acad. Sci. U. S. A.* **2014**, *111* (26), 9396−9401.

(7) Li, C.; Yue, Z.; Newstead, S.; Voth, G. A. Proton coupling and the multiscale kinetic mechanism of a peptide transporter. *Biophys. J.* **2022**, *121* (12), 2266−2278.

(8) Cui, Q.; Pal, T.; Xie, L. Biomolecular QM/MM Simulations: What Are Some of the "Burning Issues"? *J. Phys. Chem. B* **2021**, *125* (3), 689−702.

(9) Hu, H.; Yang, W. Free Energies of Chemical Reactions in Solution and in Enzymes with Ab Initio Quantum Mechanics/Molecular Mechanics Methods. *Annu. Rev. Phys. Chem.* **2008**, *59* (1), 573−601.

(10) Knight, C.; Lindberg, G. E.; Voth, G. A. Multiscale reactive molecular dynamics. *J. Chem. Phys.* **2012**, *137* (22), 22A525.

(11) Lee, S.; Liang, R.; Voth, G. A.; Swanson, J. M. J. Computationally Efficient Multiscale Reactive Molecular Dynamics to Describe Amino Acid Deprotonation in Proteins. *J. Chem. Theory Comput.* **2016**, *12* (2), 879−891.

(12) Yamashita, T.; Peng, Y.; Knight, C.; Voth, G. A. Computationally Efficient Multiconfigurational Reactive Molecular Dynamics. *J. Chem. Theory Comput.* **2012**, *8* (12), 4863−4875.

(13) Li, C.; Voth, G. A. Accurate and Transferable Reactive Molecular Dynamics Models from Constrained Density Functional Theory. *J. Phys. Chem. B* **2021**, *125* (37), 10471−10480.

(14) Agmon, N. The Grotthuss mechanism. *Chem. Phys. Lett.* **1995**, *244* (5), 456−462.

(15) Voth, G. A. Computer Simulation of Proton Solvation and Transport in Aqueous and Biomolecular Systems. *Acc. Chem. Res.* **2006**, *39* (2), 143−150.

(16) Liang, R.; Swanson, J. M. J.; Madsen, J. J.; Hong, M.; DeGrado, W. F.; Voth, G. A. Acid activation mechanism of the influenza A M2 proton channel. *Proc. Natl. Acad. Sci. U. S. A.* **2016**, *113* (45), E6955.

(17) Liang, R.; Swanson, J. M.; Peng, Y.; Wikström, M.; Voth, G. A. Multiscale simulations reveal key features of the proton-pumping mechanism in cytochrome c oxidase. *Proc. Natl. Acad. Sci. U. S. A.* **2016**, *113* (27), 7420−7425.

(18) Liang, R.; Swanson, J. M. J.; Wikström, M.; Voth, G. A. Understanding the essential proton-pumping kinetic gates and decoupling mutations in cytochrome c oxidase. *Proc. Natl. Acad. Sci. U. S. A.* **2017**, *114* (23), 5924.

(19) Lee, S.; Swanson, J. M.J.; Voth, G. A. Multiscale Simulations Reveal Key Aspects of the Proton Transport Mechanism in the ClC-ec1 Antiporter. *Biophys. J.* **2016**, *110* (6), 1334−1345.

(20) Lee, S.; Mayes, H. B.; Swanson, J. M. J.; Voth, G. A. The Origin of Coupled Chloride and Proton Transport in a Cl−/H+ Antiporter. *J. Am. Chem. Soc.* **2016**, *138* (45), 14923−14930.

(21) Wang, Z.; Swanson, J. M. J.; Voth, G. A. Modulating the Chemical Transport Properties of a Transmembrane Antiporter via Alternative Anion Flux. *J. Am. Chem. Soc.* **2018**, *140* (48), 16535−16543.

(22) Mayes, H. B.; Lee, S.; White, A. D.; Voth, G. A.; Swanson, J. M. J. Multiscale Kinetic Modeling Reveals an Ensemble of Cl−/H+ Exchange Pathways in ClC-ec1 Antiporter. *J. Am. Chem. Soc.* **2018**, *140* (5), 1793−1804.

(23) Li, C.; Yue, Z.; Espinoza-Fonseca, L. M.; Voth, G. A. Multiscale Simulation Reveals Passive Proton Transport Through SERCA on the Microsecond Timescale. *Biophys. J.* **2020**, *119* (5), 1033−1040.

(24) Ma, X.; Li, C.; Martinson, A. B.; Voth, G. A. Water-Assisted Proton Transport in Confined Nanochannels. *J. Phys. Chem. C* **2020**, *124* (29), 16186−16201.
(25) Galib, M.; Duignan, T. T.; Misteli, Y.; Baer, M. D.; Schenter, G. K.; Hutter, J.; Mundy, C. J. Mass density fluctuations in quantum and classical descriptions of liquid water. *J. Chem. Phys.* **2017**, *146* (24), 244501.
(26) Marsalek, O.; Markland, T. E. Quantum Dynamics and Spectroscopy of Ab Initio Liquid Water: The Interplay of Nuclear and Electronic Quantum Effects. *J. Phys. Chem. Lett.* **2017**, *8* (7), 1545−1551.
(27) Ceriotti, M.; Fang, W.; Kusalik, P. G.; McKenzie, R. H.; Michaelides, A.; Morales, M. A.; Markland, T. E. Nuclear Quantum Effects in Water and Aqueous Systems: Experiment, Theory, and Current Challenges. *Chem. Rev.* **2016**, *116* (13), 7529−7550.
(28) Markland, T. E.; Ceriotti, M. Nuclear quantum effects enter the mainstream. *Nature Reviews Chemistry* **2018**, *2* (3), 0109.
(29) Zuchniarz, J.; Liu, Y.; Li, C.; Voth, G. A. Accurate pKa Calculations in Proteins with Reactive Molecular Dynamics Provide Physical Insight Into the Electrostatic Origins of Their Values. *J. Phys. Chem. B* **2022**, *126* (38), 7321−7330.
(30) Chen, H.; Ilan, B.; Wu, Y.; Zhu, F.; Schulten, K.; Voth, G. A. Charge delocalization in proton channels, I: the aquaporin channels and proton blockage. *Biophysical journal* **2007**, *92* (1), 46−60.
(31) Wu, Y.; Ilan, B.; Voth, G. A. Charge delocalization in proton channels, II: the synthetic LS2 channel and proton selectivity. *Biophysical journal* **2007**, *92* (1), 61−69.
(32) Knight, C.; Voth, G. A. The Curious Case of the Hydrated Proton. *Acc. Chem. Res.* **2012**, *45* (1), 101−109.
(33) Calio, P. B.; Li, C.; Voth, G. A. Resolving the Structural Debate for the Hydrated Excess Proton in Water. *J. Am. Chem. Soc.* **2021**, *143* (44), 18672−18683.
(34) Torrie, G. M.; Valleau, J. P. Nonphysical sampling distributions in Monte Carlo free-energy estimation: Umbrella sampling. *J. Comput. Phys.* **1977**, *23* (2), 187−199.
(35) Laio, A.; Parrinello, M. Escaping free-energy minima. *Proc. Natl. Acad. Sci. U. S. A.* **2002**, *99* (20), 12562−12566.
(36) Laio, A.; Gervasio, F. L. Metadynamics: a method to simulate rare events and reconstruct the free energy in biophysics, chemistry and material science. *Rep. Prog. Phys.* **2008**, *71* (12), 126601.
(37) Invernizzi, M.; Parrinello, M. Rethinking Metadynamics: From Bias Potentials to Probability Distributions. *J. Phys. Chem. Lett.* **2020**, *11* (7), 2731−2736.
(38) Invernizzi, M.; Piaggi, P. M.; Parrinello, M. Unified Approach to Enhanced Sampling. *Physical Review X* **2020**, *10* (4), 041034.
(39) Fu, H.; Shao, X.; Chipot, C.; Cai, W. Extended Adaptive Biasing Force Algorithm. An On-the-Fly Implementation for Accurate Free-Energy Calculations. *J. Chem. Theory Comput.* **2016**, *12* (8), 3506−3513.
(40) Dama, J. F.; Parrinello, M.; Voth, G. A. Well-Tempered Metadynamics Converges Asymptotically. *Phys. Rev. Lett.* **2014**, *112* (24), 240602.
(41) Pomès, R.; Roux, B. Free energy profiles for H+ conduction along hydrogen-bonded chains of water molecules. *Biophysical journal* **1998**, *75* (1), 33−40.
(42) Chakrabarti, N.; Tajkhorshid, E.; Roux, B. t.; Pomès, R. Molecular basis of proton blockage in aquaporins. *Structure* **2004**, *12* (1), 65−74.
(43) König, P.; Ghosh, N.; Hoffmann, M.; Elstner, M.; Tajkhorshid, E.; Frauenheim, T.; Cui, Q. Toward theoretical analyis of long-range proton transfer kinetics in biomolecular pumps. *J. Phys. Chem. A* **2006**, *110* (2), 548−563.
(44) Brewer, M. L.; Schmitt, U. W.; Voth, G. A. The formation and dynamics of proton wires in channel environments. *Biophys. J.* **2001**, *80*, 1691.
(45) Li, C.; Swanson, J. M. J. Understanding and Tracking the Excess Proton in Ab Initio Simulations; Insights from IR Spectra. *J. Phys. Chem. B* **2020**, *124* (27), 5696−5708.
(46) Pezeshki, S.; Lin, H. Adaptive-partitioning QM/MM for molecular dynamics simulations: 4. Proton hopping in bulk water. *J. Chem. Theory Comput.* **2015**, *11* (6), 2398−2411.
(47) Truhlar, D. G.; Garrett, B. C.; Klippenstein, S. J. Current status of transition-state theory. *J. Phys. Chem.* **1996**, *100* (31), 12771−12800.
(48) Schenter, G. K.; Garrett, B. C.; Truhlar, D. G. Generalized transition state theory in terms of the potential of mean force. *J. Chem. Phys.* **2003**, *119* (12), 5828−5833.
(49) Dietschreit, J. C. B.; Diestler, D. J.; Hulm, A.; Ochsenfeld, C.; Gómez-Bombarelli, R. From free-energy profiles to activation free energies. *J. Chem. Phys.* **2022**, *157* (8), 084113.
(50) Roux, B. Transition rate theory, spectral analysis, and reactive paths. *J. Chem. Phys.* **2022**, *156* (13), 134111.
(51) Zinovjev, K.; Tuñón, I. Quantifying the limits of transition state theory in enzymatic catalysis. *Proc. Natl. Acad. Sci. U. S. A.* **2017**, *114* (47), 12390.
(52) Roy, S.; Schenter, G. K.; Napoli, J. A.; Baer, M. D.; Markland, T. E.; Mundy, C. J. Resolving Heterogeneous Dynamics of Excess Protons in Aqueous Solution with Rate Theory. *J. Phys. Chem. B* **2020**, *124* (27), 5665−5675.
(53) Mazzuca, J. W.; Schultz, C. P. Quantum Mechanical Enhancement of Rate Constants and Kinetic Isotope Effects for Water-Mediated Proton Transfer in a Model Biological System. *J. Phys. Chem. A* **2017**, *121* (4), 819−826.
(54) Parker, J. L.; Li, C.; Brinth, A.; Wang, Z.; Vogeley, L.; Solcan, N.; Ledderboge-Vucinic, G.; Swanson, J. M. J.; Caffrey, M.; Voth, G. A.; et al. et al., Proton movement and coupling in the POT family of peptide transporters. *Proc. Natl. Acad. Sci. U. S. A.* **2017**, *114* (50), 13182.
(55) Pedersen, B. P.; Kumar, H.; Waight, A. B.; Risenmay, A. J.; Roe-Zurz, Z.; Chau, B. H.; Schlessinger, A.; Bonomi, M.; Harries, W.; Sali, A.; et al. et al., Crystal structure of a eukaryotic phosphate transporter. *Nature* **2013**, *496* (7446), 533−536.
(56) Pao, S. S.; Paulsen, I. T.; Saier, M. H., Jr Major facilitator superfamily. *Microbiology and molecular biology reviews* **1998**, *62* (1), 1−34.
(57) Nakajima, H.; Hagting, A.; Kunji, E.; Poolman, B.; Konings, W. N. Cloning and functional expression in Escherichia coli of the gene encoding the di-and tripeptide transport protein of Lactobacillus helveticus. *Applied and environmental microbiology* **1997**, *63* (6), 2213−2217.
(58) Parker, J. L.; Li, C.; Brinth, A.; Wang, Z.; Vogeley, L.; Solcan, N.; Ledderboge-Vucinic, G.; Swanson, J. M.; Caffrey, M.; Voth, G. A.; et al. Proton movement and coupling in the POT family of peptide transporters. *Proc. Natl. Acad. Sci. U. S. A.* **2017**, *114* (50), 13182−13187.
(59) Wang, Z.; Swanson, J. M. J.; Voth, G. A. Local conformational dynamics regulating transport properties of a Cl−/H+ antiporter. *J. Comput. Chem.* **2020**, *41* (6), 513−519.
(60) Wang, D.; Voth, G. A. Proton Transport Pathway in the ClC Cl−/H+ Antiporter. *Biophys. J.* **2009**, *97* (1), 121−131.

https://doi.org/10.1021/acs.jpcb.2c06703
J. Phys. Chem. B 2022, 126, 10452−10459